Deterioration of Portland Cement-Based Materials in Low-Temperature Seawater
低温海水がセメントの耐久性に及ぼす影響に関する研究

Mari Kobayashi, Keisuke Takahashi

This study is based on a paper published in Materials 2023, 16 (15).
本報告は Materials 16 (15) に掲載された論文に基づいたものである。

Cementitious materials have potential for infrastructure development in low-temperature marine environments, including in seawater at high latitudes and in deep-sea environments (water depths of >1000 m) . Although the marine deterioration of cementitious materials has been widely investigated, the influence of seawater temperature has not been elucidated. In this study, to determine the effects of low-temperature seawater on the durability of cementitious materials, cement paste specimens were immersed in a seawater tank at room temperature and 2 ℃ for 433 days. The specimen immersed in low-temperature seawater exhibited significant deterioration with a partially collapsed surface, and Ca dissolution was more pronounced near the surface of the specimen. Such significant deterioration can be attributed to the increased solubility of portlandite under low-temperature conditions, which could promote Ca dissolution and subsequently lead to C– (A–) S–H decalcification and the formation of M– (A–) S–H and thaumasite. These insights are expected to contribute to the successful construction and maintenance of cementitious structures in low-temperature seawater.

Keywords: Deep sea, Seawater attack, Thaumasite,
Scanning Electron Microscopy - Energy Dispersive Spectroscopy (SEM-EDS)

深海での海洋技術ブレークスルーを達成するため、将来的に深海でのインフラ構築にセメント系材料が利用される可能性が考えられる。セメント系材料の海水劣化は多く研究されているが、温度影響に焦点を当てた研究はなく、水深約 1000m以上の低温海水環境におけるセメント系材料の耐久性を調査する必要がある。本研究では、ポルトランドセメントを使用したペースト試験体を２℃の海水に 433 日間浸漬させ、その耐久性を評価した。その結果、低温海水に浸漬した試験体は表層が崩壊するなどの著しい劣化を示し、さらにその表層では Ca の溶脱が顕著であることが確認された。低温条件下では水酸化カルシウムの溶解度が上昇することで、Ca の溶脱が促進され、続いてカルシウムシリケート水和物の脱灰、マグネシウムシリケート水和物やソーマサイト (Thaumasite) が生成し、表層から崩壊が進行したと考えられた。本研究結果は、深海環境下のみならず、低温海水中でのコンクリート構造物の建設や維持管理に貢献するものと期待される。

キーワード：深海、海水劣化、ソーマサイト、走査型電子顕微鏡エネルギー分散型X線分析装置 (SEM-EDS)

1 Introduction

It is well-known that approximately 70% of the earth’s surface is covered by ocean. In terms of volume, approximately 95% of the total ocean volume constitutes the “deep sea,” which is deeper than 200 m. Characteristics of the deep-sea environment are shown in Fig. 1. Because sunlight cannot reach beyond the depths of 200–500 m, photosynthesis is not possible. Furthermore, the hydraulic pressure increases at a rate of 0.1 MPa every 10 m. The water temperature of deep-sea environment is lower than that of the shallow-sea.

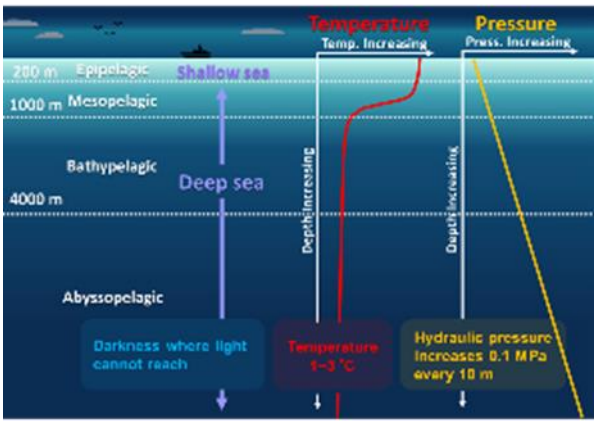

Fig. 1　Deep-sea environment.

Deep-sea exploration has been actively conducted so far, and as a result, many marine resources have been discovered. Recently in mining development as trials to obtain seabed resources have been launched[(1)-(3)]. In addition, carbon dioxide storage under the seafloor is being investigated. Such kind of technological breakthrough require the establishment of infrastructures in deep-sea environment.

Cement can be a base material for infrastructure in deep-sea environment. However, very few studies have investigated the durability of cementitious materials under deep sea conditions. In our first trial, exposure test of mortar specimens with Portland cement (PC) were conducted at a depth of 1680 m and constant temperature of the seawater at this depth was 4 °C[(4)]. The result showed that the specimens exposed for 608 days appear to be more severely damaged, and significant Ca dissolution near the surface was observed (Fig. 2). This result suggests that deterioration of PC specimen could be promoted under deep-sea condition.

Low-temperature seawater is suspected as a cause of promoted PC deterioration in deep-sea. In this study, the effect of low temperature environment on PC durability was investigated by using PC paste specimen.

2　Experimental

PC with no limestone added was used for the paste specimens. The paste was mixed using a mechanical mixer at 700 rpm for 2 minutes and cast into a 40 × 40 × 160 mm³ mold. The water-to-cement ratio was 0.6. After 28 days of curing under sealed condition at 20 °C, the specimens were immersed in room- and low-temperature seawater chamber. Room temperature seawater refers to seawater in a laboratory where room temperature was not precisely controlled. The temperature of low-temperature seawater was controlled by a thermos-controller to be at 2 ± 1 °C. Fresh seawater was always supplied to each tank at a rate of 150 ml/min, which replaced the seawater in the tank approximately every 24 hours. (Fig. 3). The specimens were immersed in each tank for 433 days.

After the immersion test, each specimen was sliced into two pieces with a thickness of 10 mm using a table bench saw with liquid paraffin, as

Fig. 2　Map of locations where exposure tests were conducted (left) , mortar specimens exposed in deep-sea for 608 days (middle) [(4)], and SEM montage image of cross-section from the specimen (right) .

shown in Fig. 4. For analysis by electron probe micro analyzer (EPMA) (JXA-8200, JEOL, Ltd.),

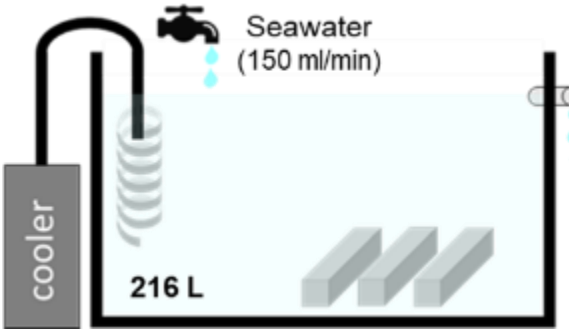

Fig. 3 Experimental set-up of seawater circulation chamber. Fresh seawater was always supplied to each tank at a flow rate of 150 ml/min.

one sample was impregnated with epoxy resin, polished, and coated with carbon. After EPMA, the sample was cut into 20 × 20 × 10 mm^3 pieces and polished again for scanning electron microscopy–energy-dispersive X-ray spectroscopy (SEM-EDS) (JSM-IT-300, JEOL Resonance) analysis. The other sample was cut using a low-speed cutter (IsoMet Cutter, Buhler) into 2 mm slices from the surface to a depth of 10 mm, and the remaining sample was denoted as the bulk sample. Mashy collapsed areas on the surface of the specimen immersed in low-temperature seawater were collected directly and denoted as the collapsed surface sample. Each piece was treated with

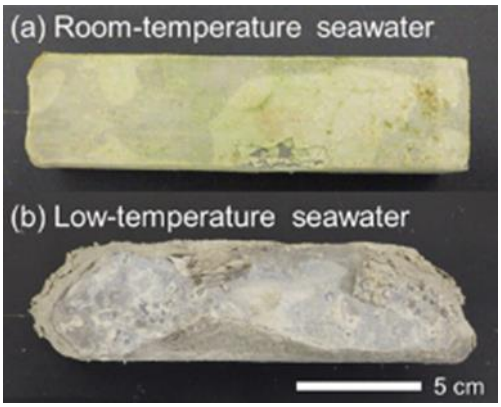

Fig. 5 PC paste specimens immersed in room-temperature seawater (a) and in low-temperature seawater (b) after 433 days.

isopropanol to stop hydration and pulverized to less than 90 μm for X-ray diffraction (XRD) (D2 PHASER diffractometer, Bruker AXS) measurement.

3 Result

Figure 5 shows the paste specimens after immersion in seawater in the laboratory for 433 days. The specimen immersed in room-temperature seawater was not significantly damaged, although the surface was covered with white precipitates of brucite. Conversely, the specimen immersed in low-temperature seawater exhibited significant surface deterioration. The specimen was partially collapsed, did not maintain its original shape, and had a fragile and mashy structure.

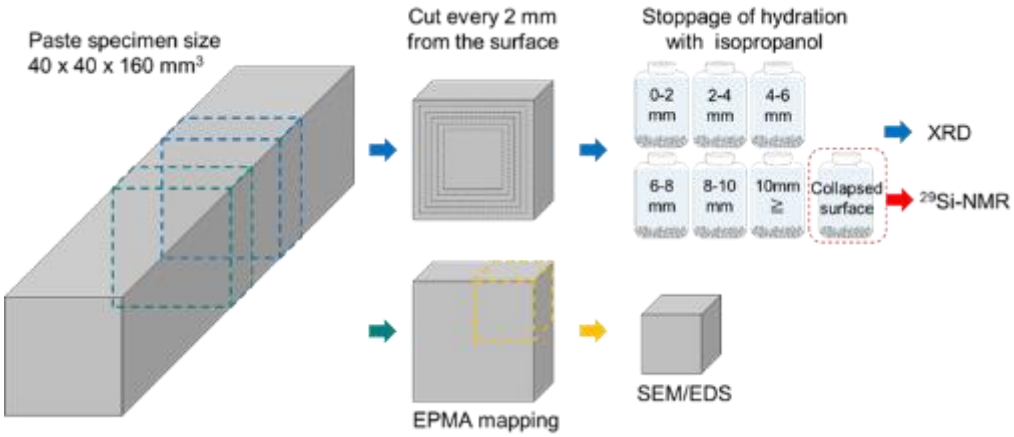

Fig. 4 Preparation of paste specimens for analysis following seawater immersion. The dotted lines indicate the cutting planes.

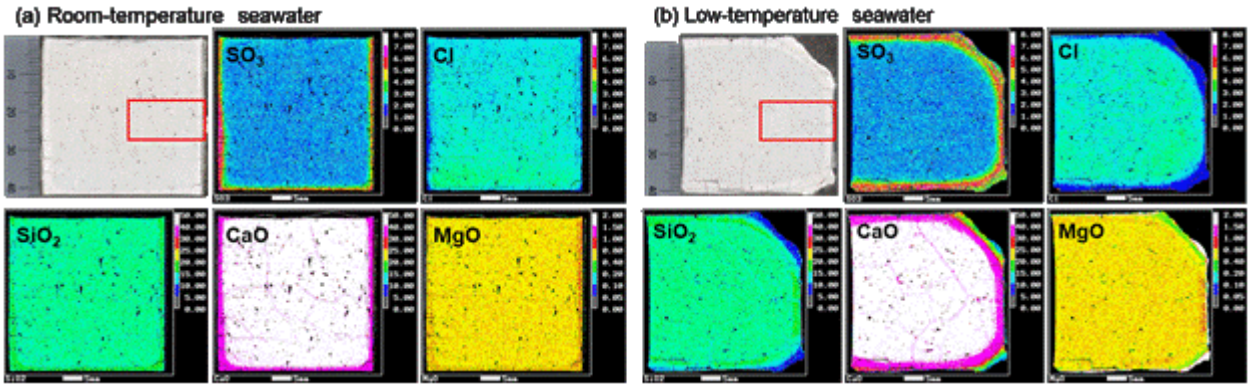

Fig. 6　EPMA elemental maps of the PC paste specimens immersed in (a) room-temperature seawater and (b) low-temperature seawater.

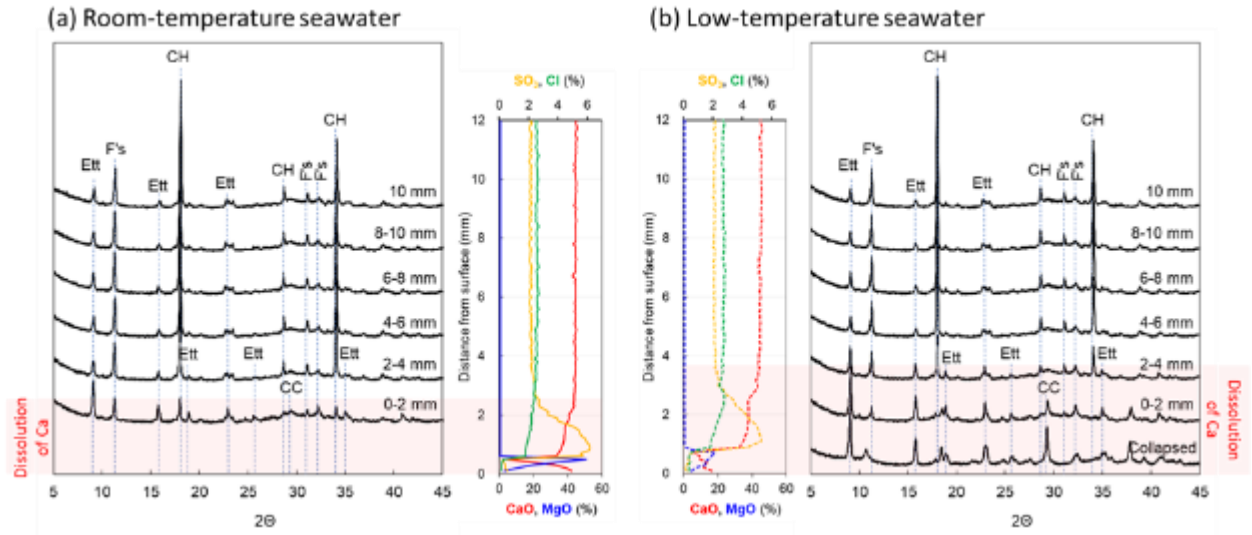

Fig. 7　XRD patterns and concentration profiles of element in the specimens obtained after immersion in (a) room-temperature and (b) low-temperature seawater. The profiles of elements are plotted from the surface (0 mm) to a depth of 12 mm within the area enclosed by the red square in Fig. 6. Ett: ettringite, F's: Friedel's salt, CH: portlandite, CC: calcite.

The results of elemental maps for each specimen, measuring the diffusion of ions from seawater and the associated dissolution of ions from cement hydrate, are presented in Fig. 6. In the case of the specimen immersed in room-temperature seawater, changes in chemical composition were observed exclusively on the surface (Fig. 6 (a)). However, for the specimen immersed in low-temperature seawater, significant changes in chemical composition were evident at greater depths (Fig. 6 (b)). Notably, Ca dissolution and SO_4^{2-} diffusion fronts were observed within the low-temperature specimen. Additionally, in the corner area where the specimen experienced collapse, there were markedly lower Ca concentrations and higher Mg concentrations. This heightened Mg concentration suggests the formation of a Mg phase, a topic that will be discussed in greater detail based on the results from EDS.

Concentration profiles for each element were analyzed from the surface (0 mm) to the interior (20 mm) of the area enclosed by the red square in the cross-sectional photographs found in Figs. 6 (a) and (b). These profiles, extending from the surface to a

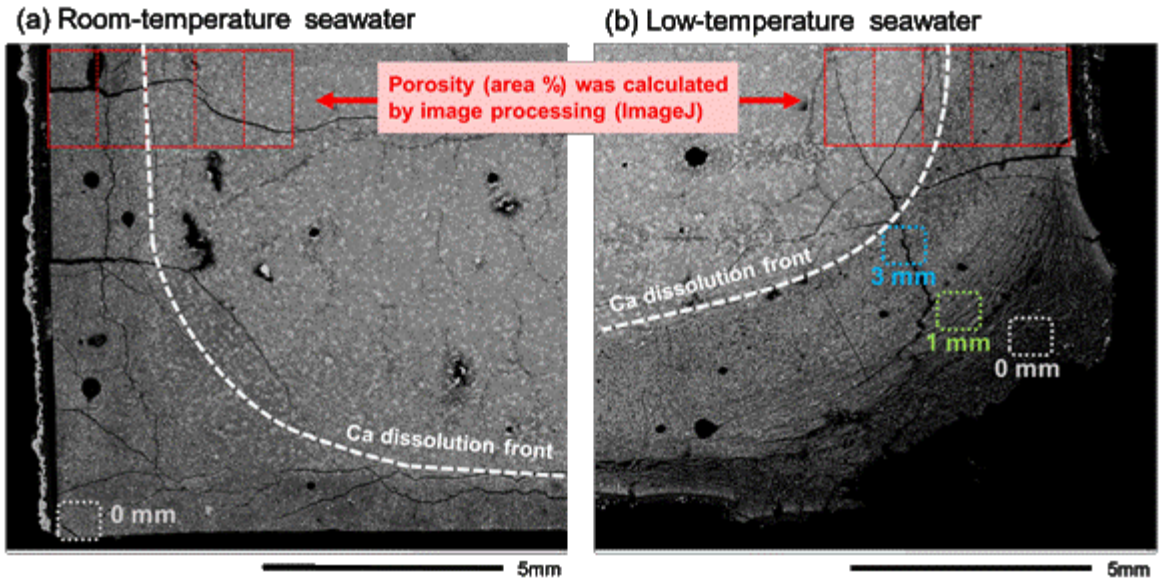

Fig. 8 SEM montage images of the specimens after immersion in (a) room-temperature seawater and (b) low-temperature seawater. The area surrounded by the red box was analyzed and calculated the porosity by image processing.

depth of 12 mm, are depicted in Fig. 7, alongside the XRD results. The profiles reveal that the Ca dissolution fronts are situated at approximately 2 mm and 3 mm for the samples immersed in room-temperature and low-temperature seawater, respectively, as determined from the Ca concentration profiles. The XRD patterns of the sample immersed in room-temperature seawater at a depth of 0–2 mm, and those of the sample immersed in low-temperature seawater at depths of 0–2 mm and 2–4 mm (corresponding to the Ca leaching area), exhibit very small portlandite peaks. This observation suggests that portlandite underwent dissolution, leaving smaller amounts of portlandite in these regions. Therefore, it can be concluded that portlandite dissolution was notably increased by immersing the specimens in low-temperature seawater. Thaumasite could also form in the collapsed surface, however, it is difficult to confirm the formation of thaumasite using XRD because of the similar structures of thaumasite and ettringite, both of which exhibit characteristic peaks at $2\theta = 9°$, 16°, and 23°. The obtained ^{29}Si NMR spectra confirmed the presence of the thaumasite phase in collapsed surface (see section 3.6 in the original paper).

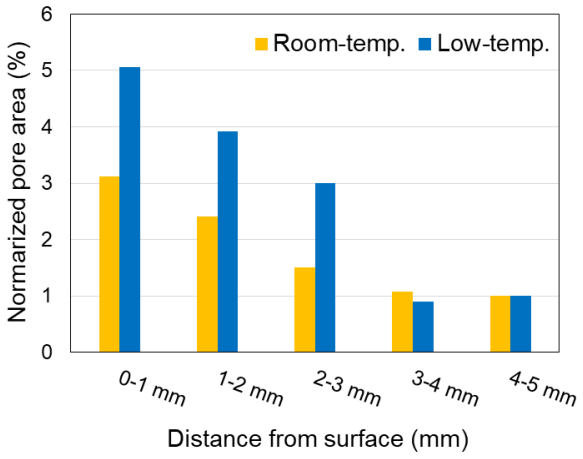

Fig. 9 Porosity (area %) of the specimens immersed in room- and low-temperature seawater.

The SEM montages in Fig. 8 reveal a grayscale change from the surface to the interior of each sample due to hydrate dissolution, indicating Ca dissolution mainly. Each SEM montage image was analyzed in 1 mm sections from the surface to the interior of the specimen in the area surrounded by the red box, and the porosity (area %) was calculated by image processing (Fig. 9). This analysis reveals that more pores existed close to the surface in both specimens. Compared with the

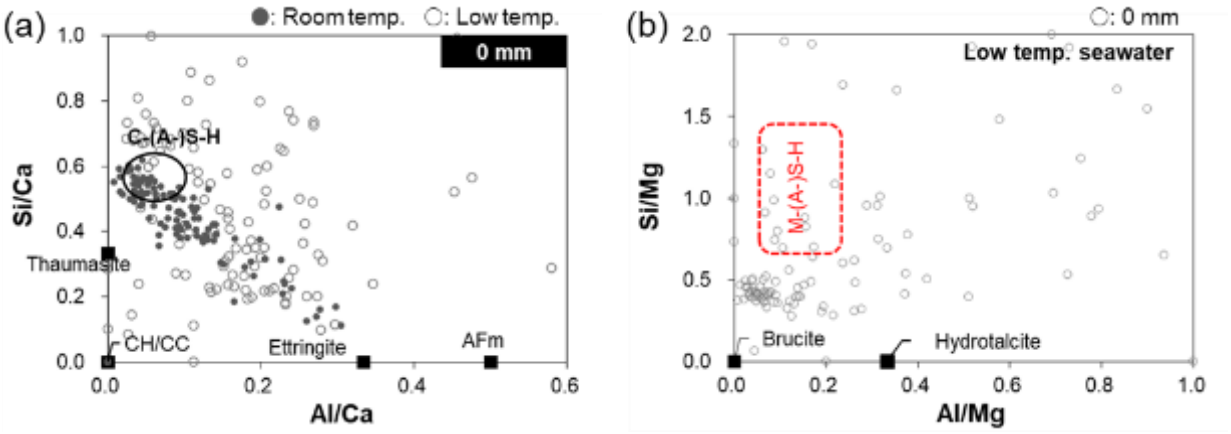

Fig. 10 EDS analysis result in atomic ratio (a) Si/Ca vs. Al/Ca at 0 mm depth from specimens immersed room- and low- temperature seawater, and (b) Si/Mg vs. Al/Mg at 0 mm depth from specimen immersed low-temperature seawater.

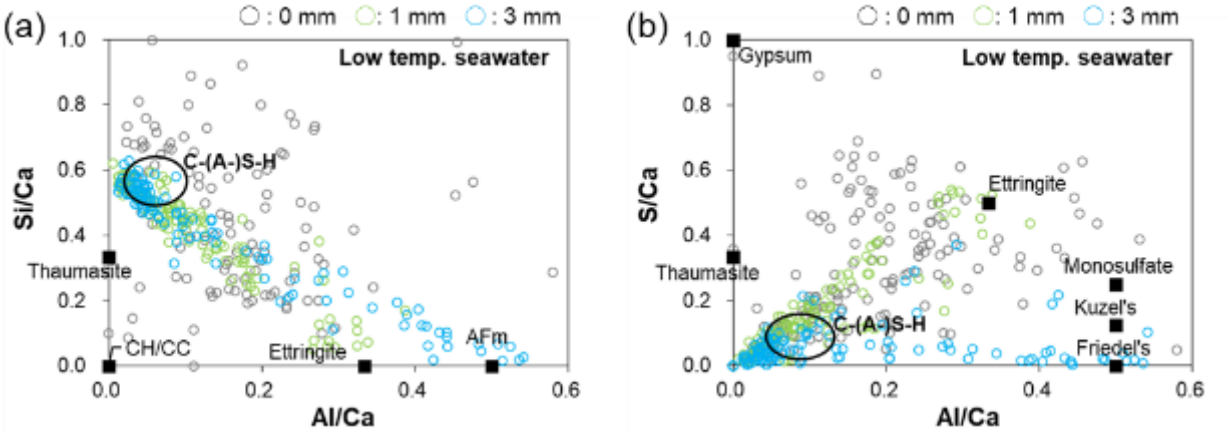

Fig. 11 (a) Si/Ca vs. Al/Ca, (b) S/Ca vs. Al/Ca at different depths from specimen immersed low-temperature seawater.

specimen immersed in room-temperature seawater, that immersed in low-temperature seawater tended to have more pores and microcracks at the same depth, indicating that hydrate dissolution was more pronounced. Based on the EPMA and XRD results, the dissolved hydrate is mainly portlandite (Fig. 6 and 7).

In Fig. 10 (a), the Si/Ca ratio is shown as a function of the Al/Ca ratio near the specimen surface (0 mm depth), determined by EDS point analysis of the specimens immersed in room- and low-temperature seawater. The circle represents the typical C–(A–)S–H composition of ordinary PC, as widely reported in the literature[5)-7)]. For the specimen immersed in room-temperature seawater, the absence of data points near the origin suggests the absence of portlandite due to portlandite dissolution. The data points do not scatter within the circled area corresponding to a typical C–(A–)S–H composition, indicating that C–(A–)S–H has not yet been decalcified. Additionally, the data points align along a trajectory toward the theoretical composition of ettringite, indicating the presence of ettringite formed by SO_4^{2-} derived from seawater. In contrast, for the specimen immersed in low-temperature seawater, the data points are more scattered and located outside the circle corresponding to a typical C–(A–)S–H composition, suggesting either C–(A–)S–H decalcification or the precipitation of new hydrates, such as Mg-based

hydrates. Furthermore, in conjunction with the XRD results (Fig. 7), the presence of some data points near the origin indicates the precipitation of calcite instead of portlandite.

Figure 10 (b) shows the relative Si and Al atomic ratios concerning the Mg content at a depth of 0 mm. The area enclosed by the red dotted line indicates the range of possible M–S–H and magnesium aluminosilicate hydrate (M–A–S–H) compositions [8]. Some data points are located in this area indicate the formation of M–S–H or M–A–S–H. Additionally, a cluster occurs outside this area, near Si/Mg = 0.5, which indicates the intermixing of M–(A–)S–H and other Mg phases (likely brucite based on the XRD results).

Figure 11 (a) shows plots of the Si/Ca ratio as a function of the Al/Ca ratio at depths of 0, 1, and 3 mm for the specimen immersed in low-temperature seawater. Portlandite is dissolved at both 1 and 3 mm considering no data points appear near the origin. The decalcification of C–(A–)S–H was observed at a depth of 0 mm, many data points were located in the C–(A–)S–H circle at depths of 1 and 3 mm. This indicates that C–(A–)S–H decalcification could not have occurred. Ettringite is formed in the 1 mm depth and Friedel's salt in the 3 mm depth (Fig. 11 (b)), indicating that phase change of hydrates from the surface to the interior are almost identical to those reported for marine deterioration before[9]-[11].

4 Discussion

The specimen immersed in low-temperature seawater showed more significant degradation than that immersed in room-temperature seawater. The temperature affects the durability of cementitious materials; for example, SO_4^{2-} attack is accelerated at low temperatures owing to the increased solubility of portlandite at low temperatures and the weakening of the surface layer owing to the formation of thaumasite[12]. The solubility of portlandite in cement increases at lower temperatures[13]. The saturation concentration of Ca^{2+} in portlandite was 1.08 times higher at 2 °C than at 20 °C[14], and more portlandite can dissolve in low-temperature environments. A steeper Ca^{2+} concentration gradient between seawater and pore solution could further drive Ca dissolution. As the portlandite dissolves, the porosity increases, as shown in Fig. 9, promoting the ion diffusion in seawater into the specimen and increase portlandite dissolution. As a result, the specimen immersed in low-temperature seawater exhibits significant deterioration than the specimen immersed in room-temperature seawater.

While portlandite dissolution increases the porosity of the specimen, as illustrated in Fig. 9, it does not result in a mushy structure or surface collapse. In the specimen exposed to room-temperature seawater, no other damage was observed despite the dissolution of portlandite in the surface layer. However, portlandite dissolution does increase seawater permeability, thereby facilitating C–(A–)S–H decalcification and, ultimately, the formation of M–(A–)S–H and thaumasite. The formation of these hydrates is expected to cause the surface layer to collapse.

Furthermore, the specimen near the surface can be damaged due the formation of ettringite. Ettringite does not always lead to serious SO_4^{2-} attack in concrete, with no cracking or spalling observed in sulfur-rich zones[9],[15]. However, in the specimen immersed in low-temperature seawater, sulfur-rich zone owing to the formation of ettringite was observed near the surface at a depth of 1 mm, and fine parallel cracks appear (Fig. 11 (b)). Ettringite precipitation in smaller (typically < 20 nm) and supersaturated with respect to ettringite can cause specimen expansion[15]. The solubility of ettringite decreases at lower temperatures[16], i.e., precipitation would be more pronounced. Although the dissolution of portlandite has caused an increase in porosity, C–(A–)S–H is present in the area where ettringite is formed, and additional ettringite formation can occur in the microporosity derived from C–(A–)S–H, resulting in the collapse of the specimen surface layer.

5 Conclusion

PC paste specimens were immersed in room- and

low-temperature seawater for 433 days. The specimen immersed in low-temperature seawater underwent more pronounced deterioration than that immersed in room-temperature seawater. The deteriorated specimen immersed in low-temperature seawater exhibited the following characteristics:

- The Ca dissolution front penetrated deeper within the sample, and portlandite dissolution was more significant compared to the specimen immersed in room-temperature seawater.
- The porosity of the specimen increased as portlandite dissolved.
- On the collapsed mushy surface, C–(A–)S–H was decalcified, and Mg-based hydrates (e.g., brucite and M–(A–)S–H) and thaumasite formed.

The increased solubility of portlandite at low temperatures led to substantial Ca dissolution and subsequent deterioration through C–(A–)S–H decalcification, resulting in the formation of M–(A–)S–H and thaumasite, ultimately resulting in the weakening and collapse of the surface. Therefore, low temperature seawater could mainly contribute to PC deterioration under deep-sea condition. As alternative binders to PC, one with less or no portlandite would be better. Suitable candidates would be calcium aluminate cement and magnesium binders, as well as binders with inorganic additives, such as fly ash and silica fume, which consume portlandite in the hydration process and create denser structure.

References

(1) E. Araki et al.: “Recurring and triggered slow-slip events near the trench at the Nankai Trough subduction megathrust,” Science, vol. 356, no. 6343, pp. 1157–1160 (2017)

(2) R. Sharma,: “Environmental Issues of Deep-Sea Mining,” Procedia Earth and Planetary Science, vol. 11, pp. 204–211 (2015)

(3) K.A. Miller, et al.: “An overview of seabed mining including the current state of development, environmental impacts, and knowledge gaps,” Frontiers in Marine Science, vol. 4 (2018)

(4) M. Kobayashi et al.: “Physicochemical properties of the Portland cement-based mortar exposed to deep seafloor conditions at a depth of 1680 m,” Cement and Concrete Research, vol. 142, p. 106335 (2021)

(5) K. De Weerdt et al.: “Changes in the phase assemblage of concrete exposed to sea water,” Cement and Concrete Composites, vol. 47, pp. 53–63 (2014)

(6) I. G. Richardson: “The nature of C-S-H in hardened cements,” Cement and Concrete Research, vol. 29, no. 8, pp. 1131–1147 (1999)

(7) P. Faucon et al.: “Aluminum incorporation in calcium silicate hydrates (C−S−H) depending on their Ca/Si ratio,” The Journal of Physical Chemistry B, vol. 103, no. 37, pp. 7796–7802 (1999)

(8) E. Bernard et al.: “Aluminum incorporation into magnesium silicate hydrate (M-S-H) ,” Cement and Concrete Research, vol. 128, p. 105931 (2020)

(9) U. H. Jakobsen et al.: “Elemental zonation in marine concrete,” Cement and Concrete Research, vol. 85, pp. 12–27 (2016)

(10) K. De Weerdt et al.: “Comparing chloride ingress from seawater and NaCl solution in Portland cement mortar,” Cement and Concrete Research, vol. 115, pp. 80–89 (2019)

(11) K. De Weerdt and H. Justnes: “The effect of sea water on the phase assemblage of hydrated cement paste,” Cement and Concrete Composites, vol. 55, pp. 215–222 (2015)

(12) M. M. Rahman and M. T. Bassuoni, “Thaumasite sulfate attack on concrete: Mechanisms, influential factors and mitigation,” Construction and Building Materials, vol. 73, pp. 652–662 (2014)

(13) R. S. Boynton: Chemistry and Technology of Lime and Limestone, second Edition. WILEY-Interscience, New York, USA (1980)

(14) Calcium hydroxide, ChemBK. Available online: https://www.chembk.com/en/chem/Calcium%20hydroxide

(15) M. Santhanam et al.: “Differentiating seawater and groundwater sulfate attack in Portland cement mortars,” Cement and Concrete Research, vol. 36, no. 12, pp. 2132–2137 (2006)

(16) B. Lothenbach et al.: “Thermodynamic modelling of the effect of temperature on the hydration and porosity of Portland cement,” Cement and Concrete Research, vol. 38, no. 1, pp. 1–18 (2008)

小林真理・こばやし　まり
研究所　セメント研究室
セメントグループ　研究員

高橋恵輔・たかはし　けいすけ
研究所　セメント研究室
セメントグループ　主幹